JOURNAL OF MATERIALS SCIENCE 16 (1981) 2745–2752

Elastic recovery at hardness indentations

B. R. LAWN, V. R. HOWES
Department of Applied Physics, School of Physics, University of New South Wales, Kensington, NSW 2033, Australia

The mechanics of hardness indentation are considered. On the basis of a cycle in which the loading is elastic–plastic and the unloading (and subsequent reloading) elastic, an expression is derived for the relative depth recovery of the impression as a function of hardness/modulus, H/E. Experimental observations on indented surfaces of selected materials, mostly ceramics, using a tilting procedure in the scanning electron microscope to measure the residual depths, confirm the predicted trends. The analysis offers a simple means of characterizing the deformation properties of materials and should provide a basis for evaluating a range of contact-related properties, particularly surface damage phenomena in sharp-particle impact.

1. Introduction

When a sharp indenter is loaded onto a flat test specimen it leaves a residual surface impression. A convenient measure of the material hardness may then be obtained by dividing the peak contact load by the projected area of the impression [1]. It is clear that hardness thus defined may be taken as an indicator of the irreversible deformation processes which characterize the test material. What is not so obvious is that this same quantity must also depend to some extent on the *reversible* deformation processes. For, the indentation stresses, although highly concentrated in the plastic region immediately surrounding the contact, may nevertheless extend at a significant level into the more remote elastic matrix. That is, hardness is strictly an elastic–plastic parameter [2]. A manifestation of this is the fact that impacting particles, sharp or otherwise, tend always to rebound from a target surface with non-zero velocity. The mechanics of hardness indentation are accordingly of considerable interest in the context of materials evaluation; apart from providing insight into the nature of the deformation itself, they bear strongly on the susceptibility to attendant microcrack generation [3, 4], with consequent relevance to strength degradation [5] and wear and erosion [6] of brittle solids.

One way in which the relative importance of reversible and irreversible components of contact deformation might be expected to be evident is in the elastic recovery during unloading of the indenter. Studies of impression geometries in metallic and non-metallic materials using various standard microhardness indenters indicate that whereas characteristic in-surface dimensions generally remain a reasonably faithful measure of those at maximum loading (thereby justifying a definition of hardness in terms of post-indentation measurements) the depth does not [7, 8]. Extremes in depth recovery are shown by "soft" metals, where it is negligible, and "highly elastic" rubbers, where it is nearly complete. Typically brittle materials, e.g. ceramics, which are of primary interest in this work, will be seen to occupy the "middle ground". The question therefore arises as to how the indentation recovery may be quantified in terms of well-defined elastic–plastic parameters, in a form which suitably characterizes the material response.

The present paper seeks to answer this question by developing a formulation for the degree of elastic recovery as a function of a basic hardness/modulus ratio, H/E. It is to be noted that both H and E are macroscopic parameters which are readily measurable without explicit knowledge of micromechanical processes. In this sense our approach is somewhat phenomenological and can therefore provide little insight into the mechanisms (as opposed to the mechanics) of indentation

0022–2461/81/102745–08$02.80/0

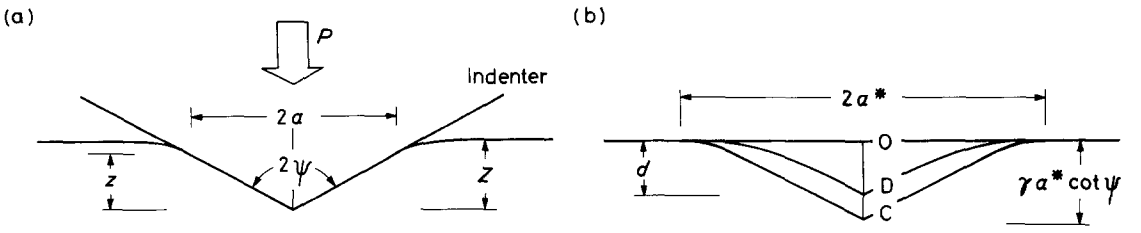

Figure 1 Contact geometry, showing co-ordinate system: (a) at intermediate load P; (b) at extremes of indentation, zero load (0), maximum load (C) and complete unload (D).

deformation. At the same time it avoids the extreme complication which inevitably attends any attempt at a detailed elastic–plastic stress analysis [9]. Depth measurements of residual impressions left by Vickers indentations in a range of selected materials provide confirmation of the basic theoretical predictions. The results bear strongly on impulsive loading phenomena and suggest that the hardness/modulus ratio may be taken as a useful indicator of a given material's incapacity to absorb impact energy.

2. Mechanics of indentation cycle

Consider a rigid, fixed profile indenter of regular geometry with respect to the axis of loading, i.e. cone or pyramid, pressed into a flat test surface, as in Fig. 1a. Then the depth of the indenter tip below the contact perimeter may be written as $z = a \cot \psi$, where a is a characteristic contact "diameter" and ψ is a corresponding indenter semi-angle. For instance, with a Vickers indenter a is generally measured as an impression half-diagonal, whence (by definition) $\psi = \arctan (7/2) = 74.05°$ is the semi-angle between opposite pyramidal edges. The actual penetration of the indenter below the specimen surface is denoted by Z, which will differ from z if the contact perimeter is depressed (as shown in Fig. 1) or elevated. We may take this into account by writing $Z = \gamma z$, where γ is a geometrical factor, in which case

$$Z = \gamma a \cot \psi \qquad (1)$$

becomes the governing relation for penetration in terms of a and ψ.

The object of the exercise now is to determine how the penetration varies with applied contact load P through the indentation cycle, i.e. we require the function $P(Z)$. Not only does this function hold the key to the degree of depth recovery, its integral directly determines the mechanical energy input associated with the indentation process. Our first step to this end is to introduce the mean contact pressure, p_0, i.e. the normal force divided by the projected constant area, into the description; then, with the aid of Equation 1, we may write

$$P = p_0 \alpha_0 a^2 = [p_0(\alpha_0/\gamma^2) \tan^2 \psi] Z^2, \qquad (2)$$

where α_0 is another geometrical factor ($\alpha_0 = 2$ for a Vickers indenter). Thus for any conditions under which the terms within the square bracket on the right-hand side of Equation 2 remain invariant, the load is quadratic in penetration. This form of dependence was first discussed in relation to the problem of elastic recovery, for the special case of conical intenders, by Stilwell and Tabor [8], whose paper stands as an important precursor to the present work. Our analysis builds on that of these earlier workers in two major respects: first, we develop the formalism in terms of the basic H/E parameter, so that materials evaluation may be more convenient; second, we incorporate a residual-field term to allow for the post-indentation configuration representing a significant departure from that of the initial, flat test surface.

Let us now consider the loading–unloading indentation cycle in two separate stages, with reference to Fig. 1b for the boundary conditions:

(i) *Loading half-cycle.* During loading the material deforms in a complex elastic–plastic mode. A well-established, simplifying feature of this deformation is the geometrical similarity which characterizes the associated stress and displacements fields [1]. In terms of Equation 2, this means that the composite square-bracket factor is independent of P, provided the given material is homogeneous. In this case the mean contact pressure is a constant of the material, and thereby affords a useful measure of hardness, i.e. $p_0 = H =$ constant. The parameter γ must also remain constant under these conditions, and, provided the plastic material immediately surrounding the contact zone does not "pile-up" or "sink-in" to any great extent (a proviso which is

expected to prevail in harder materials, such as ceramics [9]), should not differ much from unity. Thus, over the loading path OC in Fig. 1b, from the initial surface configuration at $Z = 0$ to the maximum penetration at $Z = Z^* = \gamma a^* \cot \psi$, the controlling material parameter in the deformation mechanics is the hardness H. Accordingly, for this stage of the indentation cycle Equation 2 may be written with the dependent variables and parameters in an appropriately subscripted form,

$$P = [H(\alpha_0/\gamma_H^2) \tan^2 \psi] Z_H^2. \quad (3)$$

(ii) *Unloading half-cycle.* The existence of a residual impression means that the $P(Z)$ curve must show some hysteresis on unloading. However, this hysteresis largely disappears after one complete cycle: subsequent reloading retraces the unloading path CD to good approximation [8]. (Upon reloading beyond the first maximum load point the indentation must, of course, revert to the original load path.) Thus the unloading occurs elastically. The similitude principle may be applied as before, but, as will be seen below, bears somewhat closer scrutiny. For the mean contact pressure we follow Stilwell and Tabor [8] and make use of the solution of Sneddon [10] for a rigid cone in contact with an elastic half-space, giving $p_0 = (E \cot \psi)/2(1 - \nu^2)$, where E is Young's modulus and ν is Poisson's ratio. According to Sneddon's analysis, the parameter γ has the value $\pi/2$, although in the context of the present problem we shall have occasion to regard this as something of an overestimate. Now, since this stage of the indentation process is essentially reversible, we may usefully treat the problem in terms of the reloading mechanics. This raises an important point concerning the boundary conditions; it must be recognized, in accordance with Equation 2, that it is the surface configuration at $Z = 0$ which corresponds to our zero-stress reference origin. Stilwell and Tabor [8] took the tip of the unloaded impression as their reference origin, effectively translating their depth co-ordinate along the load axis, but this ignores the fact that any such configuration which departs from that of the initial flat surface necessarily exists in a state of residual stress. The situation is analogous to the loading of a precompressed spring; the true zero in the load–displacement response must be reckoned relative to the natural rather than the precompressed length, a distinction which becomes vital if the response is non-linear, as is indeed the case with our "spring", Equation 2. Thus, as a first step in the hypothetical reload sequence we proceed via the path OD in Fig. 1b, from $Z = 0$ to the residual depth $Z = Z_r = d$, to obtain a configuration "equivalent" to that of the final impression. The corresponding load for this step is $P_r = \{[E/2(1 - \nu^2)] (\alpha_0/\gamma^2) \tan \psi\} d^2$, which may be regarded as the precompression force. It is, of course, at this point that the *actual* loading in the real indentation situation begins, so the "effective" contact force acting over the path DC in Fig. 1b is $P = P_E - P_r$, where $P_E(Z_E)$ is the elastic deformation function of Equation 2 for a surface with no residual impression (i.e. for the "spring" without precompression). We thus have within the range $Z_r \leqslant Z_E \leqslant Z^*$, in analogy to Equation 3,

$$P = \{[E/2(1 - \nu^2)] (\alpha_0/\gamma_E^2) \tan \psi\} (Z_E^2 - Z_r^2). \quad (4)$$

The condition for compatibility of the two half-cycles is that at the maximum load $P = P^*$ the penetrations should be equal, $Z_H = Z^* = Z_E$. Thus from Equations 3 and 4 we obtain

$$(Z_r/Z^*)^2 = 1 - [2(1 - \nu^2)(\gamma_E/\gamma_H)^2 \tan \psi] H/E. \quad (5)$$

Accordingly, for a given indenter geometry the relative depth recovery is effectively determined by the hardness/modulus parameter, H/E (the Poisson's ratio term $(1 - \nu^2)$ varying by a relatively small amount from material to material). It should be noted that the ratio Z_r/Z^* in Equation 5 remains independent of the peak contact load.

The way in which we have incorporated the notion of a residual force into the analysis needs further elaboration here. From Equation 2 we have immediately that $P_r/P^* = (Z_r/Z^*)^2$, so that, depending on the value of H/E, P_r may be an appreciable fraction of P^*. That the intensity of the residual stress field around indentations can be substantial is well known, both from direct observations of the associated bi-refringence in transport materials [11, 12] and from the effect such fields can have in driving indentation cracks long after unloading is complete [5, 12]. In this interpretation, the end-point in the indentation process could equally well be achieved in Fig. 1 via the elastic–plastic load–unload route OCD or the simple elastic load route OD (assuming in the latter case that the onset of irreversible processes could be suppressed by some means). However, the implied equivalence of these two routes cannot

TABLE I Hardness and modulus of materials tested

Material	Source	H/(GPa)	E/(GPa)
Soda-lime glass	Commercial sheet	5.6	70
Glass ceramic (Pyroceram C9606)	Corning Glass	8.4	109
Si_3N_4 (NC132)	Norton	18.5	300
Al_2O_3 (AD999)	Coors Porcelain	20.1	406
MgF_2 (Irtran)	Kodak	7.3	170
WC (Co-bonded)	NBS	12.7	575
Steel ("soft")	Zwick	1.62	200
Steel ("hard")	Zwick	7.7	200

be complete. To see why not, we recall Equation 1, which, in the notation used above, yields $a_E/a_H = \gamma_H/\gamma_E$ for the relative surface contact dimension at the same depth $Z_H = Z = Z_E$ during the loading (OC) and reloading (DC) half-cycles. In general, and specifically in the vicinity of $Z = Z_r$, we expect that γ_H and γ_E will necessarily differ, because the deformation processes are themselves different. But as Z approaches Z^* we must expect the two γ terms to tend to the same value, for compatibility arguments it is required that $a_H = a_E$ at the peak loading. Hence, on the presumption that the constancy of γ_H is not at issue [1], the validity of the similitude principle in the elastic reloading sequence must be questioned. Nevertheless, observations in tests on metals that the $P(Z)$ function does follow a near quadratic unloading–reloading curve [8] provide some justification for taking the present formulation as a reasonable first approximation.

3. Measurements of elastic recovery

3.1. Materials preparation and indentation procedure

In order to test the validity of the theory, experimental measurements of depth recovery were made at residual impressions in selected materials. Table I lists the selection, together with values of H and E. The fact that most of the materials are ceramics reflects our own interest in intrinsically brittle solids; two steels are included in the study for limited comparison purposes, but polymeric materials, because of their complex time-dependent mechanical properties, are avoided. The hardness and modulus were determined routinely for each material, H directly from the impression dimensions as the mean contact pressure and E from the elastic deflections on instrumented, four-point bend specimens. An accuracy of better than 5% was obtained for each of these two quantities. It is seen from Table I that the values of H/E cover a reasonably wide range. Each material was prepared with a flat, mirror-smooth test surface, using 1 μm diamond paste to produce the final finish.

For the indentation procedure, a standard Vickers hardness testing facility was used. The inherent rigidity of the diamond indenter and the well-defined indentation pattern that results (particularly at the pyramidal tip and edges) in the specimen surface are ideally suited to recovery determinations. The materials were each indented over a range of peak contact loads, limited in each case by the threshold for radial cracking [3, 13]; this limitation, imposed to avoid complications due to pattern disruption, meant that the residual impression depth was small, typically $\approx 1\,\mu$m for most of the ceramics.

3.2. Measurement of impression depth

To measure the degree of recovery, a simple but sensitive procedure was devised whereby the impressions were viewed at oblique incidence in a scanning electron microscope. This technique was useful for even the smallest impression depths, where optical techniques (including interferometry) were ineffective. The procedure involved tilting the indented surface with respect to the image plane about an axis containing one of the impression diagonals, thereby producing a foreshortening of the other, mutually orthogonal diagonal. Examples of the patterns obtained are shown in Fig. 2, for soda-lime silicate glass. It can be seen that the tips and corners of the pyramidal impressions are well defined in the micrographs, in spite of some curvature at the edges.

Fig. 3 illustrates the geometrical principles involved in the recovery evaluation. For a normal image plane the Vickers indentation has four-fold symmetry, with half-diagonals of length a^*. This orientation, of course, provides no information on the depth d of the impression. For an oblique image plane, at tilt angle β, the pattern is reduced

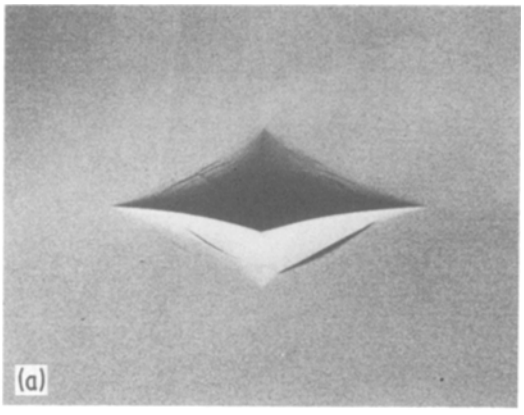

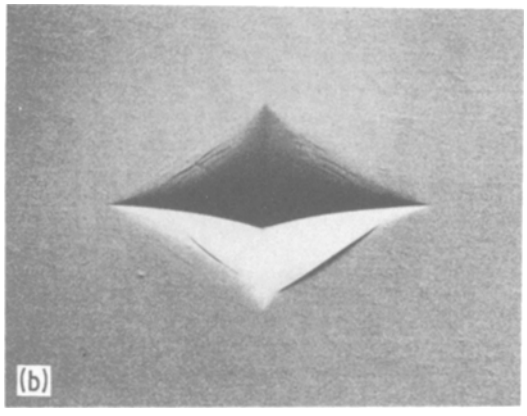

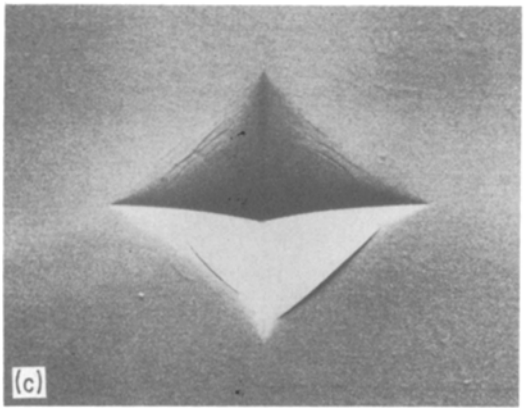

Figure 2 Scanning electron micrographs of Vickers impressions in soda-lime glass. Peak indentation load $P^* = 2N$, half-diagonal about tilt axis (horizontal in diagram) $a^* = 13\ \mu m$. Tilt angles: (a) $\beta = 60°$, (b) $\beta = 50°$, (c) $\beta = 35°$. (Minor cracking is evident at this impression.)

to two-fold symmetry, with apparent half-diagonals a_1^* and a_2^* perpendicular to the tilt axis. We now have from the diagram

$$a_2^* + a_1^* = 2a^* \cos\beta \qquad (6a)$$

$$a_2^* - a_1^* = 2d \sin\beta. \qquad (6b)$$

Elimination of β then gives

$$d/a^* = [(a_2^* - a_1^*)/2a^*]/\{1 - [(a_2^* + a_1^*)/2a^*]^2\}^{1/2}. \qquad (7)$$

Thus the ratio of residual depth to impression half-diagonal may be obtained from simple, comparative measurements on the micrographs, independent of the indentation load and the tilt angle.

Determinations of d/a^* were accordingly made for each of the materials listed in Table I. In each case an evaluation was made from 15 to 25 micro-

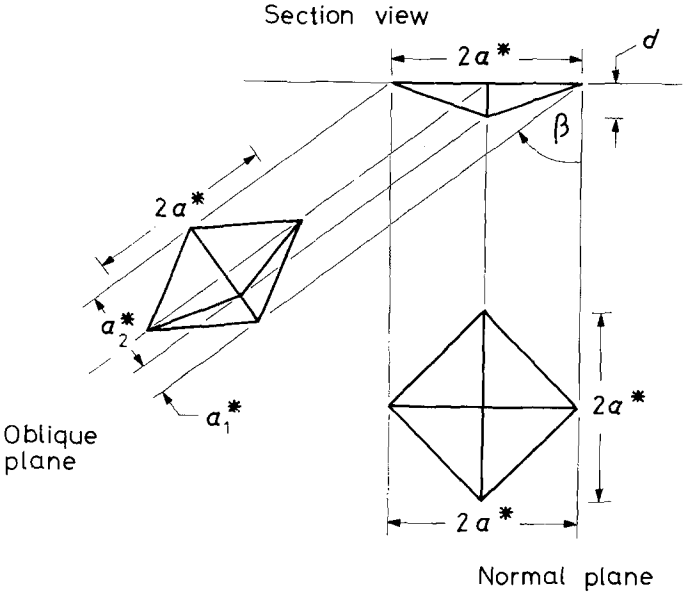

Figure 3 Schematic diagram showing geometry of impression depth measurement technique. Diagram shows projection of impression topography onto normal and oblique image planes.

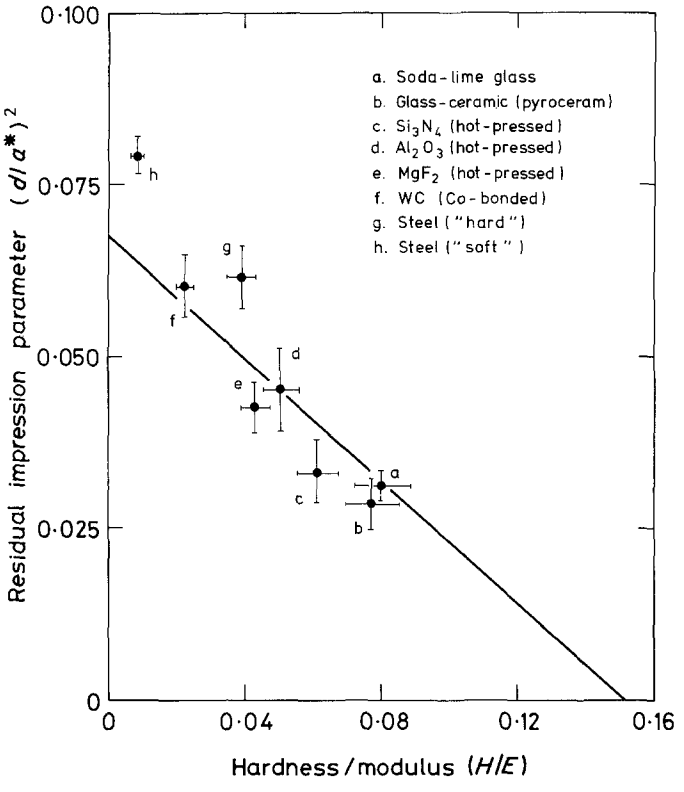

Figure 4 Plot showing measured residual depth parameter $(d/a^*)^2$ as a function of H/E for materials listed in Table I.

graphs, representing different indentations, loads, tilt angles and tilt axes (the last to average out any systematic error arising from non-symmetry in the indentation process itself). Bearing in mind that the most accurate estimates of d/a^* from Equation 7 will come from micrographs for which the pattern distortion is greatest (note that as we approach the configuration of normal incidence, such that for $\beta \to 0$, $a_1^* \approx a^* \approx a_2^*$ in Equation 6, the uncertainty in the evaluation will tend to infinity), the mean value and standard deviation for each material was computed in accordance with an appropriate weighting procedure. This procedure consisted of assigning a weight equal to the inverse square of the experimental error for each individual determination from Equation 7, consistent with the uncertainty in half-diagonal measurements on the micrographs.*

For those less brittle materials tested (i.e. the steels and the WC specimens) where crack-free impressions could be produced to depths in excess of 10 μm, direct optical measurements by the depth-of-focus technique afforded a useful cross-check of the scanning electron microscopy (SEM) evaluations. Where this was possible the optical data were included in the computations of the recovery parameter, weighting the individual points in accordance with an inverse error term as before.

4. Results and discussion

If now we make the substitutions $Z_r = d$ and $Z^* = \gamma a^* \cot \psi$, along with the approximation $\gamma_H \approx \gamma \approx \gamma_E$ (Section 2), in Equation 5, we obtain

$$(d/a^*)^2 = \gamma^2 \cot^2 \psi - [2(1-\nu^2)\gamma^2 \cot \psi]H/E, \quad (8)$$

which provides us with the necessary basis for analysing the results. Accordingly, Fig. 4 shows a plot of $(d/a^*)^2$ against H/E. The data points represent the experimental determinations; the vertical error bars denote standard deviations (as determined in Section 3), and the horizontal error bars a nominal error of 10% in the hardness/modulus ratio. The solid line is a best-fit of Equation 8 to the data, obtained by taking $\nu = 0.25$ (a representative value for the materials considered) and $\psi = 74.05°$ (Vickers), and by making the adjustment $\gamma = 0.91 \pm 0.08$ (mean and standard deviation averaged over all materials).

*See any text on statistical methods.

Fig. 4 may be regarded as a graphical indicator of the position occupied by the different materials in the elastic–plastic spectrum, i.e. between the extremes of ideal elasticity ($d/a^* = 0$, $H/E = (\cot\psi)/2(1-\nu^2) = 0.15$) and ideal plasticity ($d/a^* = \gamma\cot\psi = 0.26, H/E = 0$).

In assessing the agreement between theory and experiment in Fig. 4 it is as well to remember the assumptions which characterize the model. We have already mentioned the necessary departure from load invariance of at least one of the γ terms, in Section 2, and the consequent violation of the underlying similitude principle. This uncertainty in the value of γ is compounded by the fact that we have been dealing with a pyramidal rather than a conical indenter; for instance, how justified is the use of Sneddon's solution for axially symmetric loading to derive Equation 4. In addition, we have taken the indenter to be rigid throughout, whereas in reality the effective semi-angle ψ will tend to a somewhat larger value, depending on the deformability of the specimen material (as characterized by H and E) relative to that of diamond. Further, it has been postulated (with some empirical justification from other sources) that all loading hysteresis disappears after the first cycle; the occurrence of reversed plasticity is not uncommon in elastic–plastic problems, however, and a proper analysis would need to examine this possibility more closely [14]. These are all facets of the analysis which call for a detailed study of the complete $P(Z)$ response for individual materials. Our limited study of post-indentation configurations, while providing all the pertinent information needed for a quantitative evaluation of recovery, allows us only to investigate the boundary conditions of the problem.

It is important to reiterate that our analysis deals strictly with the mechanics of indentation, and not the mechanisms. Equation 8 is useful in the light it throws on the proportions of reversible and irreversible deformation associated with the hardness parameter, and, as such, affords a convenient basis for materials evaluation. As mentioned in Section 1, this type of information may be of critical importance in the determination of a wide range of contact-related properties, particularly in brittle solids, but the formulation tells us nothing explicit about the nature of the actual deformation processes at the micromechanical level. It is possible that different deformation mechanisms may have some influence on the similitude parameter γ in Equation 8; indeed, the tendency in Fig. 4 for the data points representing the metallic materials to lie above those representing the ceramics may be a manifestation of a somewhat different deformation geometry. However, such effects are likely to be of secondary importance only, with all the more essential details of the micromechanical response concealed within the macroscopic parameters H and E.

5. Implications in impact loading

It is of some interest to examine the implications of the theoretical development in Section 2 concerning impact phenomena. We deal here with impact velocities much less than the speed of sound waves in solids, in order that a quasistatic approximation may be applied. Also, we neglect possible sources of energy dissipation (e.g. flexural vibrations, losses at specimen supports) other than within the immediate contact zone itself.

Suppose that a sharp indenter is incident onto a target surface with initial kinetic energy, U_K^i, and rebounds with final kinetic energy, U_K^f. Then noting that the kinetic energy must be zero at maximum penetration and neglecting any changes in gravitational potential energy during the contact, we may use work/energy principles to obtain

$$U_K^i = \int_0^{Z^*} P(Z_H)\,dZ_H = \tfrac{1}{3}P^*Z^* \qquad (9a)$$

for the loading half-cycle, using Equation 3 to evaluate the work integral, and

$$U_K^f = \int_{Z_r}^{Z^*} P(Z_E)\,dZ_E = \tfrac{1}{3}P^*Z^*[(1-3Z_r^2/Z^{*2} + 2Z_r^3/Z^{*3})/(1-Z_r^2/Z^{*2})] \qquad (9b)$$

for the unloading half-cycle (written here in terms of the work to reload the system), using Equation 4. Combination of Equations 9a and 9b allows us to determine an expression for the coefficient of restitution in terms of the residual depth parameter Z_r/Z^*, or, in conjunction with Equation 5, of the material parameter H/E;

$$e = (U_K^f/U_K^i)^{1/2} = \{(1-3Z_r^2/Z^{*2} + 2Z_r^3/Z^{*3})/(1-Z_r^2/Z^{*2})\}^{1/2} \qquad (10a)$$

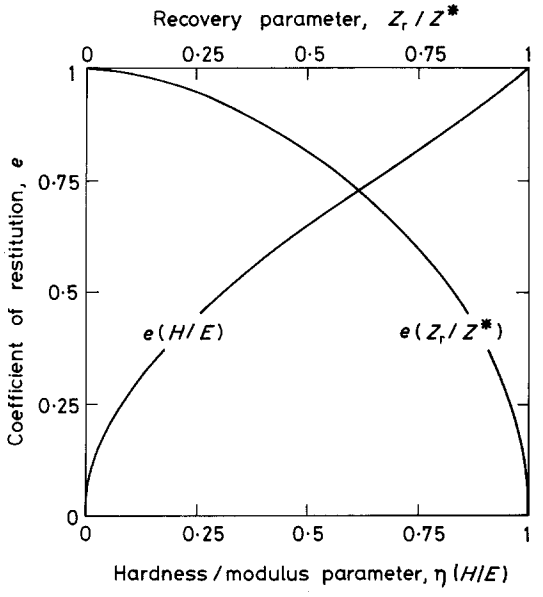

Figure 5 Graphical representation of Equations 10a and 10b, showing functional dependence of coefficient of restitution as a function of recovery parameter and hardness/modulus, respectively.

$$= \{3\eta H/E - 2[1-(1-\eta H/E)^{3/2}]/(\eta H/E)\}^{1/2}, \quad (10b)$$

where $\eta = 2(1-\nu^2)(\gamma_E/\gamma_H)^2 \tan\psi$. Thus for a given contact geometry the intrinsic coefficient of restitution is uniquely determined by the degree of recovery, which is in turn determined by the hardness/modulus ratio. A plot of Equations 10a and 10b is given in Fig. 5.

The coefficient of restitution e is, of course, a useful measure of the degree of reversibility of the contact deformation processes. The fraction of the work input expended in one complete cycle is given by $(U_K^i - U_K^f)/U_K^i = 1 - e^2$. Hence the capacity of a material to dissipate energy decreases as H/E increases. Such dissipative effects can be important in the characterization of surface damage properties in prospective sharp-particle impact situations, particularly in relation to strength degradation and erosion. They can, for instance, determine the extent of surface melting at the contact zone [15]. More importantly perhaps, they can exert an influence on the mechanics of crack initiation and propagation in the more brittle materials [4]. The potential also exists, by monitoring e as a function of contact velocity, for investigating time dependencies of the basic deformation parameters in rate-sensitive materials, including polymers.

Acknowledgements

We are grateful to D. B. Marshall for helpful comments on this study.

References

1. D. TABOR, "Hardness of Metals" (Clarendon Press, Oxford, 1951).
2. D. M. MARSH, *Proc. Roy. Soc. Lond.* A279 (1964) 420.
3. B. R. LAWN and A. G. EVANS, *J. Mater. Sci.* **12** (1977) 2195.
4. B. R. LAWN, A. G. EVANS and D. B. MARSHALL, *J. Amer. Ceram. Soc.* **63** (1980) 574.
5. D. B. MARSHALL, B. R. LAWN and P. CHANTIKUL, *J. Mater. Sci.* **14** (1979) 2225.
6. A. G. EVANS, M. E. GULDEN and M. E. ROSENBLATT, *Proc. Roy. Soc. Lond.* A361 (1978) 343.
7. H. BÜCKLE, *Metall. Rev.* 4 (1959) 49.
8. N. A. STILWELL and D. TABOR, *Proc. Phys. Soc. Lond.* 78 (1961) 169.
9. S. S. CHIANG, D. B. MARSHALL and A. G. EVANS, unpublished work (1980).
10. I. N. SNEDDON, *Proc. Cambr. Phil. Soc.* **44** (1948) 492.
11. A. ARORA, D. B. MARHSALL, B. R. LAWN and M. V. SWAIN, *J. Non-Cryst. Sol.* **31** (1979) 415.
12. D. B. MARSHALL and B. R. LAWN, *J. Mater. Sci.* **14** (1979) 2001.
13. B. R. LAWN and D. B. MARSHALL, *J. Amer. Ceram. Soc.* **62** (1979) 347.
14. R. HILL, "The Mathematical Theory of Plasticity" (Oxford University Press, London, 1950).
15. B. R. LAWN, B. J. HOCKEY and S. M. WIEDERHORN, *J. Amer. Ceram. Soc.* **63** (1980) 356.

Received 19 March and accepted 25 March 1981.